Magnetic Interactions of Neighbouring Stator Sets in Multi DOF Local Electromagnetic Actuation for Robotic Abdominal Surgery

F Leong[1], A Mohammadi[1], Y Tan[1], D Thiruchelvam [2], P Valdastri[3], D Oetomo[1]

Abstract— **This paper aims to characterise the magnetic interaction in neighbouring sets of local electromagnetic actuation (LEMA) actuators in a robotic platform for abdominal surgery. The analysis looks into the affect of the magnetic fields contributed by a stator-rotor set (the actuation unit) located adjacent to the rotor of interest. Each rotor drives one of the degree-of-freedoms (DOFs) on a surgical robotic device. In this study, a two-DOF setup is used for the magnetic interaction analysis, which can be expanded to general case *n*-DOF setup with the Principle of Superposition of magnetic fields from multiple sources. The magnetic model is then used to compute the dynamics of the system, which involves the equation of motion of the rotors and associated robotic mechanism it drives, and the actuator (electrical) model that takes into account the back EMF generated by the permanent magnet rotors. The magnetic field effect of the neighbouring set onto the rotor is observed by obtaining the speed response of the rotor through simulation so that the dynamic model can be validated against the experimental results. The outcomes are useful for the design specification of the LEMA system configuration, involving the feasible / pragmatic distance between the stator sets such that the interference is minimised, and for the design of the necessary control strategy.**

I. INTRODUCTION

Since minimally invasive surgery (MIS) was initiated in the late 1980s [1], much research and developments have been performed to improve the benefits of the surgical procedure and to further reduce surgical trauma onto patients. This led to the introduction of the laparoendoscopic single-site (LESS) surgical technique which requires only a single incision at the umbilicus for laparoscopic tools to be inserted through to gain access within the abdominal cavity [2]. Due to the rigid mechanical link on the surgical instruments, the dexterity and manoeuvrability of the instruments are severely constrained by the incision point, causing difficulties to access to multiple quadrants of the abdomen [3].

To address this constraint, it was proposed that the rigid mechanical transmission in the conventional laparoscopic device is replaced with magnetic linkages [4]. This allows the surgical tool to be fully inserted into the abdominal cavity for full intra-abdominal mobility while being completely unattached to the external unit. The mobility and anchoring of the magnetic surgical systems are made possible with magnetic coupling between the permanent magnets located within the device to be inserted internally and the permanent magnets on the external side of the abdominal wall, hence the term "magnetic anchoring and guidance system (MAGS)" [5]. Following this, many researches implemented MAGS into the development of surgical devices along with robotic manipulators driven by embedded DC micromotors [6]. Nonetheless, due to size constraint on the surgical devices for a 20mm diameter port insertion, DC micromotors that could be embedded into the devices faces an upper limit in size and therefore power, which restricts its suitability for some complex surgical manipulation [3].

To further enhance the functionality of the MAGS devices, local magnetic actuation (LMA) was then incorporated into the device to provide actuation onto surgical manipulators through magnetic coupling across the abdominal wall, i.e. magnetic spur gear [7]. Multiple prototypes of surgical manipulators have been designed and developed to implement the LMA concept [8], [9]. Electromagnet stators are tested in place of the external actuation permanent magnet stators to investigate the implementation of LMA with other magnetic sources [10], introducing the term "local electromagnetic actuation (LEMA)" (see Fig. 1). The feasibility and control of a single DOF LEMA setup with a set of electromagnetic stators and a permanent magnet rotor using the scalar control and vector control (i.e. Field Oriented Control) methods were demonstrated. This provides a good platform for LEMA to be implemented in a multi-DOF configuration, in which multiple sets of electromagnet stators with corresponding rotors are required to actuate multi-DOF surgical manipulators. For instance, two stator sets with corresponding internal permanent magnet rotors across the barrier (i.e. abdominal wall in surgical environment) to drive a two-DOF cable-driven robotic camera [11], as shown in Fig. 2. The rotor, when actuated, will rotate a spool which winds the cable pulling a linkage on the robotic manipulator for a DOF.

As multi-DOF manipulation is desired for dexterous surgical manipulation within the abdominal cavity, multiple pairs of external stators - internal rotor are required. This means that there will be a neighbouring pair(s) of LEMA to each rotor, which may introduce systematic disturbances to the operation of each individual rotor. To analyse the magnetic interactions within the LEMA setup, general magnetic and electromechanical models of the LEMA were established in [12]. These models allow arbitrary and multiple magnetic sources to be taken into consideration, enabling

[1] Florence Leong, Alireza Mohammadi, Ying Tan and Denny Oetomo are with the Melbourne School of Engineering, The University of Melbourne, 3010 Victoria, Australia. fleong@student.unimelb.edu.au, {alirezam,yingt,doetomo}@unimelb.edu.au

[2] Dhan Thiruchelvam is with the Department of Surgery, University of Melbourne at St Vincent's Hospital

[3] Pietro Valdastri is with the University of Leeds. p.valdastri@leeds.ac.uk

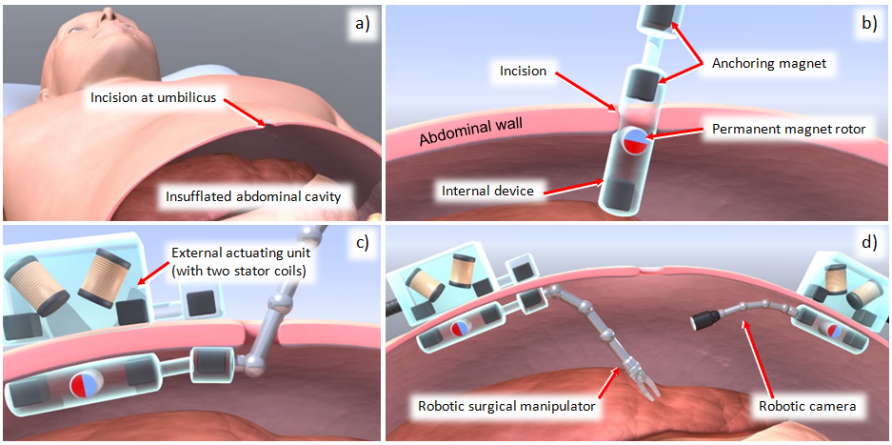

Fig. 1: Illustration of the multi-DOF LEMA system in abdominal surgery, a) an incision is made at the umbilicus of an insufflated abdomen, b) an internal surgical device connected to a multi-DOF robotic surgical tool is inserted into the abdominal cavity through the incision, c) the internal device is coupled with the respective external actuation unit on the external side of the abdominal wall using anchoring magnets, and d) more than one LEMA system can be inserted intra-abdominally to perform cooperative surgical tasks, requiring multiple neighbouring LEMA sets within the workspace of the abdomen. The prototype of the robotic camera and its actuation units in this illustration are shown in Fig. 2.

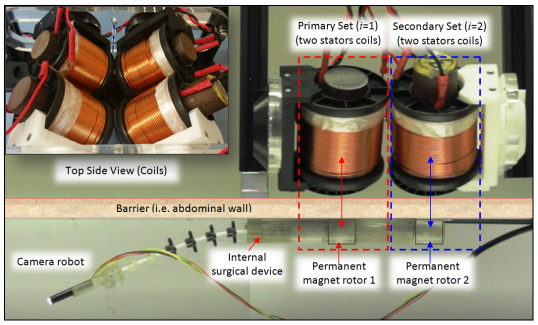

Fig. 2: A two-DOF robotic surgical camera actuated by two sets of electromagnet coil stators driving corresponding permanent magnet rotor, which is embedded inside the internal surgical device [11].

the investigation of magnetic field and torque interactions at the position of a particular rotor. The accuracy of the models was validated experimentally for static operation, with rotor attached to a lead cell for measurements of the generated electromagnetic torque.

This paper therefore extends the author's prior work on static cases and investigates the non-static rotor operation of the electromechanical system and its effects in a multi-DOF system configuration. The rotation of the rotor excites dynamics, which were not validated in the static operation reported in [12], such as the back electromotive force (EMF) due to the rotation of the rotor as well as the coil inductance due to the variance of the supply current to the coils. The effects of a neighbouring pair of LEMA on the operation of a rotor includes the magnetic interaction between two sets of stator coils onto an intended rotor, taking the dynamics of both stator sets into consideration. The dynamic model of the two-DOF system is simulated with the open loop scalar control method used in [10] to observe the interaction of the magnetic fields, and the results are then compared against experimental results for validation.

The reminder of this paper is organised as follows. Section II describes the magnetic field and electromechanical models of a two-DOF LEMA system as well as its system dynamics, taking into consideration its neighbouring stator set for the investigation of the magnetic interaction onto an actuating rotor. Section III discusses the model computational analysis and the simulation of the dynamic model presented, implementing the scalar control method to obtain the speed response of the rotor for validation against the experimental results, while the experimental setup and procedures are described in Section IV. The results with experimental validations and discussions are presented in Section V. From the study, the establishment of the equation of motion describing the dynamics of the overall LEMA system and the interactions among its various components is important for the determination of system design specification as well as the development of model-based control systems to address undesired interferences generated by external magnetic and environmental disturbances.

II. Modelling of Multi-DOF LEMA

For a surgical system to have the capability of performing various surgical tasks, a multi-DOF LEMA configuration is required to actuate a multi-DOF robotic surgical manipulator. This means that there will be neighbouring sets of LEMA units arranged within a vicinity on the external side of the abdomen. The neighbouring sets of stator-rotor LEMA units will produce systematic (undesired) magnetic interference to the rotors actuating the surgical robotic device inside the abdominal cavity. In this section, such disturbance is discussed. Note that the Principle of Superposition inherently applies to the magnetic interaction

among the sources of magnetic field. Therefore, the model of interaction between a rotor and a neighbouring source of magnetic field can be extended to any number of magnetic sources through superposition.

In this section, utilizing the magnetic model presented in [12], the magnetic field interaction of both the stator sets on rotor R_1 is analysed based on the configuration illustrated in Fig 3. The system may consists of n stators-rotor sets, with index i identifying the stator-rotor set ($i = 1,2,...,n$, e.g. $i = 1,2$ for two stators-rotor sets in a two-DOF system which is considered in this study). The rotors are denoted as R_i, with each rotor R_i driven by two actuating stators, denoted as S_{ij}, where $j = \{1,2\}$, respectively. This model can be easily expanded to cater for more DOFs in the system.

The relative pose between two stator sets in a 3D space can be represented with a homogeneous transformation matrix. However, for this paper, we assume the lateral placement of the stator sets for space saving measure. The lateral distance between two sets of stator coils, defined as the inter-set distance, is assigned by D_S.

A. Magnetic Field Model

The magnetic field at any arbitrary points around an electromagnetic coil can be obtained using the the Biot-Savart Law. In [12], an expression for the magnetic field generated by a single stator coil S_i at any arbitrary point in which the rotor R_i is located, has been derived as shown below:

$$B_q = \frac{\mu_0 \mu_r I N R_c}{4\pi} \int_{z'=l/2}^{l/2} \int_{\varphi'=0}^{2\pi} \frac{C_q}{D} d\varphi' dz' \tag{1}$$

where $q = x, y,$ and z, respectively, μ_0 and μ_r are the permeability of free space ($4\pi \times 10^7 H/m$) and the relative permeability of the core material, respectively, R_c is the radius of the coil, N is the number of turns in the coil, I is the current through the coil and

$$C_q = \begin{cases} (z\text{-}z')\cos\varphi' \hat{i}, & q = x \\ (z\text{-}z')\sin\varphi' \hat{j}, & q = y \\ (R - x\cos\varphi' - y\sin\varphi')\hat{k}, & q = z \end{cases}$$

$$D = (x^2 + y^2 + (z\text{-}z')^2 + R_c^2 - 2R_c(x\cos\varphi' + y\sin\varphi'))^{3/2} \tag{2}$$

Although this model caters for the magnetic field contributed by a single stator coil, it can be conveniently expanded to cater for the magnetic field contribution of multiple magnetic sources, as per discussed in II-B.

B. Considering Magnetic field of Multiple Stators and a Neighbouring Stator Set on a Given Rotor

The general magnetic model can be expanded to take into account multiple stator coils (i.e. $S_{ij}, j = \{1,2\}$) around R_i, as well as neighbouring sets of stators, for instance stator set 2 denoted as S_{2j}, by applying the same equation to obtain the magnetic field generated by these stators at R_i. The total effects of both stator sets, i.e. stator set 1, S_{1j} and stator set 2, S_{2j}, would be summed due to the Principle of Superposition. In Figure 3b, the schematic of two neighbouring sets of stator-rotor sets is depicted. Considering rotor R_1 in the figure, it can be seen that the rotor not only experiences the magnetic field from stator set 1, which is its intended actuation, but also that of stator set 2, which is intended to drive rotor R_2. The affect of R_2 is assumed to be negligible in this paper, especially if the alignment of the permanent magnet rotors are such that they are axially aligned.

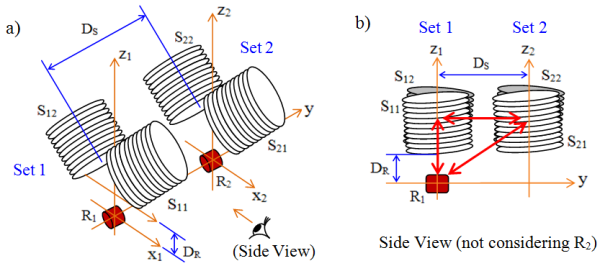

Fig. 3: A schematic diagram of the two-DOF electromagnetic LMA system, a) 3D illustration and b) side view of the system with the magnetic interactions (depicted by the red arrows) among the stator sets and the rotor, R_1, with a neighbouring rotor, R_2 being negligible.

The resultant magnetic field at rotor R_i considering the magnetic fields contribution from all sources in its vicinity (except for R_2) can be obtained as $\boldsymbol{B}_{R_i} \in \Re^3$:

$$\boldsymbol{B}_{R_i} = B_x \hat{i} + B_y \hat{j} + B_z \hat{k} \tag{3}$$

where B_x, B_y and B_z are the summations of the corresponding magnetic field components contributed by all the magnetic sources (i.e. stator coils in all sets present) in the vicinity of R_i in the Cartesian space.

C. Equation of Motion of Rotor R_i

The resultant B_{R_i} obtained will be used in the electromechanical model to determine the torque generated by the stators on rotor R_i [12] in the equations of motion below:

$$\sum \boldsymbol{\tau}_i = \boldsymbol{J}_i \ddot{\boldsymbol{\theta}}_i + \boldsymbol{b}_i \dot{\boldsymbol{\theta}}_i = \boldsymbol{\tau}_S - \boldsymbol{\tau}_{L_i} \tag{4}$$

where $\boldsymbol{J}_i \in \Re^{3\times3}$ and $\boldsymbol{b}_i \in \Re^{3\times3}$ are the total moment of inertia and the viscous friction coefficient of the permanent magnet rotor respectively, and $\boldsymbol{\theta}_i \in \Re^3$ is the rotational position of the rotor about each axis. The electromagnetic torque on rotor R_i by the all the stators, $\boldsymbol{\tau}_S \in \Re^3$ and the load torque, $\boldsymbol{\tau}_{L_i} \in \Re^3$ are expressed as:

$$\boldsymbol{\tau}_S = \boldsymbol{m}_i \times \boldsymbol{B}_{R_i} = \begin{bmatrix} -B_y m_i \cos\theta \\ -B_z m_i \sin\theta - B_x m_i \cos\theta \\ -B_y m_i \sin\theta \end{bmatrix} \tag{5}$$

$$\boldsymbol{\tau}_{L_i} = \boldsymbol{r}_i \times \boldsymbol{F}_{L_i}$$

where $\boldsymbol{F}_{L_i} \in \Re^3$ is the force exerted by the load and $\boldsymbol{r}_i \in \Re^3$ is the distance of R_i from the load, whereas $\boldsymbol{m}_i \in \Re^3$ is the magnetic moment of the rotor R_i related to the magnetization M_i and the length of the rotor h_i, with the net m_i given by:

$$m_i = \pi r_i^2 h_i M_i \tag{6}$$

hence, the resultant torque due to all stators, τ_S as follows:

$$\tau_S = \pi r_i^2 h_i M_i B_{R_i} \sin\theta_i \sin(\theta_i - \alpha) \tag{7}$$

Note that the torque generated in Eq. (5) takes into account the contributions of stator set S_{1j} and that of the neighbouring set S_{2j}.

D. Actuation Dynamics of LEMA with Coupling Back EMF from Neighbouring Stator Set

The dynamics of the LEMA system involves the magnetic and electrical interactions between the current supply to the stators and the rotor actuation. Hence, the equations of the electrical portion of the system is required, taking into account the coils inductance as the current supply varies and the back emf as the rotor rotates, resulting in varying angular position and flux linkage [10]:

$$v_{ij} = R_S i_{ij} + L\frac{di_{ij}}{dt} + e_{ij}, \tag{8}$$

where $j = \{1,2\}$ and v_{i1} and v_{i2} are the phase voltages of i^{th} stators, i_{i1} and i_{i2} are the currents through the i^{th} stators, R_S and L_S are the resistance and self-inductance of the stators, assuming the same across all stators, and e_{i1} and e_{i2} are the back-EMF voltages acting on the two coils of the i^{th} stator which can be expressed as follows:

$$\begin{aligned} e_{i1} &= \omega_i \psi_{R_i} \sin(\theta_i), \\ e_{i2} &= \omega_i \psi_{R_i} \sin(\theta_i - \alpha), \end{aligned} \tag{9}$$

where $\omega = d\theta_{R_i}/dt$ is the angular speed of rotor i, α is the angle between the stators (S_{i1} and S_{i2}) and ψ_{R_i} is the flux linkage at the rotor, R_i. Hence, the resultant torque generated by the stators can also be expressed as:

$$\tau_S = \psi_{R_i}(i_{i1}\sin(\theta_i) + i_{i2}\sin(\theta_i - \alpha)), \tag{10}$$

The comparison between Eq. 10 and the electromechanical model which applies the resultant magnetic field, B_{R_i} in Eq. 7 gives the knowledge of ψ_{R_i} to compute the back EMF for the computational analysis of the system dynamics. Note that Eq. 8 only takes into account the back EMF of stator S_{ij} generated by the motion of rotor R_i and not the neighbouring rotor. This assumption is deemed reasonable when the distance between rotors (inside the abdominal cavity), D_S is larger by at least a factor of two (geometrically) compared to the distance between the rotors and the stators, D_R (refer to Fig 3), keeping in mind the exponential decay of the magnetic field strength with distance. This is generally true for the current setup, with the average abdominal thickness of $D_R = 20mm$ while $D_S = 65mm$. The distance, D_S is determined by the bulk of the stator design.

III. Computational Analysis of Multi-DOF LEMA

To analyse the magnetic interaction in a multi-DOF LEMA setup with neighbouring stator sets, a simulation is performed by implementing the magnetic field model, the equations of motions and the system dynamics as discussed in Section II. The resultant magnetic field, taking into account the magnetic field contributed by all the stators (i.e. stator set 1 and the neighbouring stator set or stator set 2) onto the rotor, R_1 is computed using the Principle of Superposition. The resultant field is then applied into the dynamic simulation to study the behaviour of R_1 with the presence of the neighbouring stator set (stator set 2) by obtaining the speed response of R_1, in which the effect of the magnetic interference caused by stator set 2 can be seen.

A. Simulations Parameters

The computation analysis and dynamic simulation of the LEMA system are performed in Matlab and Simulink, with the incorporation of the mathematical models presented in Section II as well as the knowledge of the unknown parameters identified in (see Table I). The unknown parameters related to the dynamic electromagnetic models (i.e. R_S, L_S, b_i, and J_i) have been identified using experimental methods described in [10] and the unknown parameters required in the magnetic and static electromechanical models (i.e. μ_{r_i}, and M_i) were identified using experiments in [12].

TABLE I: Model parameters of electromagnet-based LMA

Parameters	Values	Reference
Resistance (R_S)	0.8 Ω	[10]
Inductance (L_S)	5.8 mH	[10]
Friction Coefficient (b_i)	3.9×10^{-6} Nms	[10]
Total Moment of Inertia (J_i)	6×10^{-7} kgm^2	[10]
Relative permeability of core (μ_{r_i})	5.2	[12]
Magnetization (M_i)	4.45×10^5 A/m	[12]

B. Simulations Procedures

Even though the study involves an open-loop system, the interference analysis requires the speed response of the rotor R_i, which needs to be regulated with respect to the variations in the magnitude and frequency of the voltage supply. Hence, a conventional method used in permanent magnet synchronous motors (PMSMs), the open-loop scalar control method [10] is chosen for implementation due to its simplicity for visualisation of the system response during the magnetic interaction between two sets of stator coils onto the rotor, R_1. The speed of the rotor is regulated by adjusting the magnitude of stator voltages ($V_{S_{ij}}$) and frequency ($f_{S_{ij}}$) such that the stators flux linkage is always maintained at the desired value during steady-state. At steady state, di_{i1}/dt and di_{i2}/dt in the system model (see Eq. 8) will be zero, and with the stator resistance, R_S assumed negligible, the flux linkage at the rotor, ψ_{R_i} can be expressed as:

$$V_s \cong (\psi_{pm})\omega \rightarrow \psi_{pm} \cong \frac{V_s}{2\pi f} \tag{11}$$

Keeping the ratio, $V_{S_{ij}}/f_{S_{ij}}$ constant for any change in $f_{S_{ij}}$, ψ_{R_i} will remain constant, providing constant current amplitudes, thus having the generated torque independent of the supply frequency at any time.

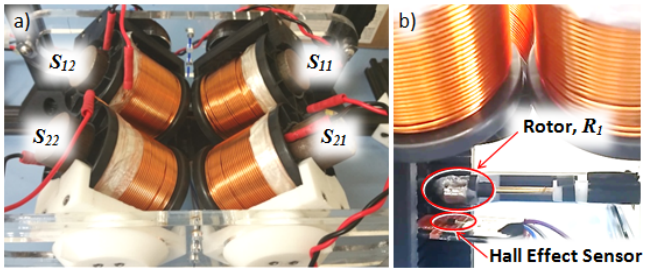

Fig. 4: Experimental setup, a) top view of the two-DOF stator pairs setup and b) side view of the experimental setup, showing rotor R_1 and the Hall Effect sensor

The simulation started with current supplied to only the stator set 1 (i.e. S_{11} and S_{12}). Stator set 2 (i.e. S_{21} and S_{22}) is then initiated after 5 seconds of the runs. This allows a direct observation of the change in the angular velocity of the rotor, maintaining a reference velocity of 60rad/s on rotor, R_1 while subjecting stator set 2 to a speed of 30rad/s and 100rad/s. The results obtained are compared with experimental results for analysis in Fig. 5 and Fig. 6 in Section V-A.

IV. Experiments

The magnetic interference contributed by a neighbouring set, i.e. stator set 2, onto rotor, R_1 based on the simulations discussed in Section III is visualised experimentally to validate the computational models presented in Section II. Similarly, the open loop scalar method described in Section III-B is employed to obtain the speed responses of the system at R_1 for comparison against the simulated results.

A. Experimental Setup

An experimental platform with two sets of stator pairs was set up to simulate the two-DOF LMA system (see Fig. 4). The stator coils are of similar specifications, with 1.32mm copper windings of 250 turns. Rotor, R_1 (a cylindrical Neodymium magnet, N42 with 9.5 mm in diameter and length) is positioned right below the stator set 1, as configured in the simulation described in Section III. The Hall Effect sensor (UGN3503UA) is placed below R_1 to provide a knowledge of the rotor angular position when it is rotating in order to compute the rotor flux linkage, ψ_{R_1} for the rotor actuation. Sabertooth 2×10 is utilised to provide dual channel supplies to the both the stator sets.

B. Experimental Procedures

The experiment is performed with the stator pairs as close as possible to one another ($D_S = 65mm$ or $2.5r_S$, where r_S is the stator coil radius of 25mm in average among all four coils, with the coil holder flange at a diameter of $32.5mm$) to simulate the worse case scenario in which the magnetic interaction would be at its largest. The rotor, R_1 is positioned 20mm below the stator coils (D_R) in relevance to an abdominal wall thickness of approximately 15mm, also such that the magnetic interaction would be more prominent. Similar to the simulation procedure, the experiment started by driving stator set 1 for 5 seconds before switching stator set 2 on to provide an observation of the interference by the magnetic interaction between the stators sets. The rotor, R_1 is expected to follow a reference velocity of 60 rad/s while the stator set 2 runs at angular velocities of 30 rad/s and 100 rad/s.

V. Results and Discussions

A. Experiment and Computational Results

The results obtained from the open loop scalar control simulation discussed in Section III and the experiments described in Section IV are presented in this section. The velocity responses of rotor R_1 obtained from the simulation and experiments, with different reference velocities assigned to the neighbouring pair of stators, are plotted together for comparison and validation of the theoretical model.

Figure 5 shows the simulation and experimental results with the reference velocity to stator set 1 at 60 rad/s and stator set 2 driven at 100 rad/s angular speed. As it is an open loop scalar control technique, an overshoot was encountered in both the simulated and experimental results at the beginning of the transient while the controller attempts to track the given reference speed at R_1 (see Fig. 5). The steady state was achieved approximately 0.7 seconds and 0.5 seconds for the simulation and experimental results,

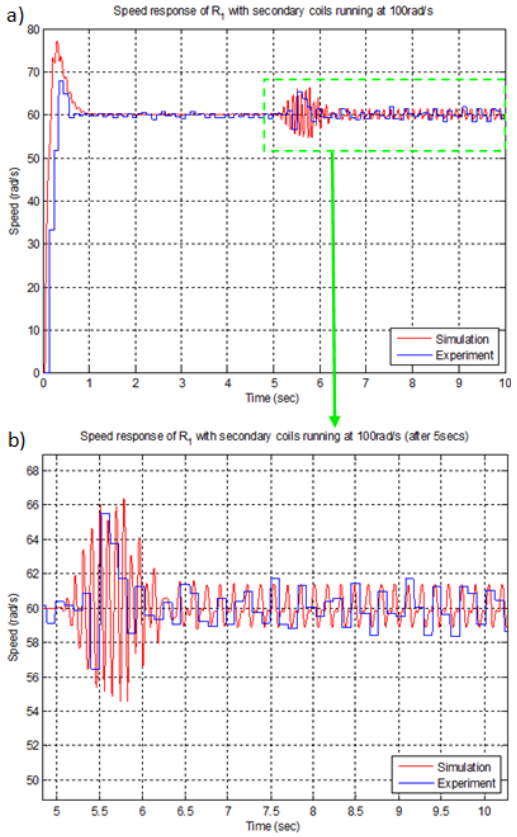

Fig. 5: a) Speed response of R_1, and b) with stator set 2, driven at 100rad/s, switched on after 5 seconds

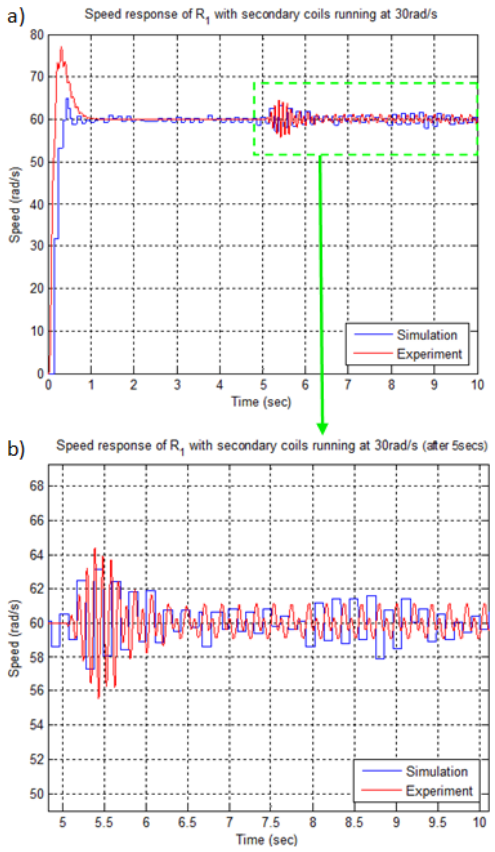

Fig. 6: a) Speed response of R_1, and b) with stator set 2, driven at 30rad/s, switched on after 5 seconds

TABLE II: Comparisons of the variance and standard deviation of the steady state response between experiment and simulated results, before and after switching on stator set 2.

Status of Set 2	Set 2 Speed Ref.	Std Dev. (σ)	Variance (σ^2)
OFF	N/A	0.4959 $\pm$ 0.05	0.2482 $\pm$ 0.05
ON	30 rad/s	1.080 $\pm$ 0.21	1.2104 $\pm$ 0.45
ON	100 rad/s	0.817 $\pm$ 0.16	0.6945 $\pm$ 0.27

respectively. There are inherently discrepancies between these two data due to some variations in the experimental setup, such as environmental noise and uncertainties. When stator set 2 was switched on, R_1 experiences the magnetic interference contributed by stator set 2. This created a transient oscillation with a range of approximately 55 rad/s to 66 rad/s in the simulation, and approximately 56 rad/s to 65.5 rad/s in the experiment (see Fig. 5b). The response reaches its steady state after about 1.5 seconds, and the amplitude of oscillation at this stage is about 1.8 rad/s for both simulation and experiment.

Likewise, similar observation was obtained with the simulation and experiment performed with stator set 2 running at 30 rad/s starting at five seconds, retaining the reference speed of R_1 at 60 rad/s throughout (see Fig. 6). The angular velocity of R_1 oscillated with the amplitude of 4 rad/s and 3.5 rad/s in the simulation and experiment respectively after switching stator set 2 on (see Fig. 6b). The response reached its steady state after 1.2 seconds, with the amplitude of the oscillations of approximately 1.1 rad/s in the simulation and approximately 1 rad/s in the experiment.

Table II shows the variance and standard deviation of the experiment data against the simulation, with speed reference at R_1 at 60 rad/s before and after switching stator set 2 on with independent speed references (i.e. 30 rad/s and 100 rad/s). These results are based on five sets of repetition runs. The interference effect on the rotor in stator set 1 can clearly be seen from the difference in the standard deviation and variance of the speed response before and after stator set 2 was switched on. The interference is observed to be different as well with difference speed references for stator set 2.

B. Discussions

From these simulations and experiments, the results from the simulated theoretical model match the experimental results well, demonstrating that the models are considerably accurate. The magnetic interference effect onto the R_1 by stator set 2 can obviously be seen with sinusoidal fluctuation in the speed response compared to the approximately constant response before stator set 2 was switched on. This effect will in turn cause an impact on the rotation of the intended rotor to perform consistent winding of the cable actuating the robotic surgical manipulator. When more than two stator sets are involved, the magnetic interference will be larger, thus the effect will be more severe. Furthermore, actuating more DOFs on the robotic manipulator with such magnetic interference would result in undesired abrupt movements during surgical tasks.

On the other hand, if the stator sets are moved further apart, the magnetic interference decreases. For instance, looking at just the responses with 60rad/s speed reference for stator set 1 and 100 rad/s speed reference for stator

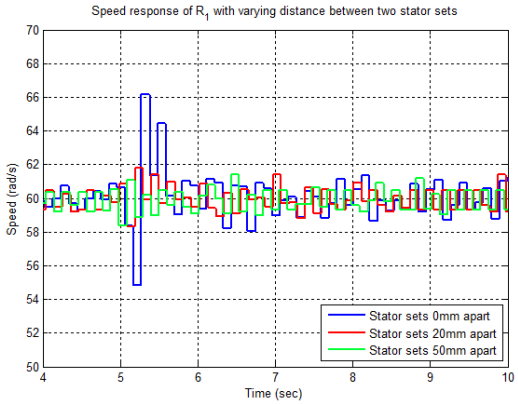

Fig. 7: Speed responses of the rotor, R_1 with 0mm ($D_S = 65mm$, according to Fig 3), 20mm ($D_S = 85mm$) and 50mm ($D_S = 115mm$) distance between stator set 1 and stator set 2 (inter-set distances), focusing only on the response when stator set 2 is switched on at 5 seconds.

TABLE III: Standard deviation and variance of the interference steady state response for inter-set distance of 0mm (D_S=65mm), 20mm (D_S=85mm) and 50mm (D_S=115mm)

Inter-set distance (mm)	Standard Dev. (σ)	Variance (σ^2)
0 (D_S=65)	0.817	0.6945
20 (D_S=85)	0.6575	0.4323
50 (D_S=115)	0.6352	0.4035

set 2, along with a distance of 20mm inter-set distance ($D_S = 85mm$), the disturbance experienced by rotor, R_1 is reduced (see Fig 7). This can be observed at the instance stator set 2 is switched on, with lesser initial fluctuation as well as lower interaction steady state deviations. When stator set 2 is moved further away from stator set 1 (i.e. inter-set distance of 50mm, $D_S = 115mm$), the interference reduction onto R_1 is observed to be insignificant as compared to that of $D_S = 85mm$. This can be seen in Table III, which shows the standard deviation and variance of the steady state interference response for each inter-set distance.

Even though complete elimination of the interference contributed by stator set 2 is desired in the system (i.e. with having the stator sets as far as possible away from each other), it has to be noted that the configuration of the system is constrained by the limitation of space above the abdominal wall, bearing in mind that there would be more than two sets involved to drive more DOFs on a robotic manipulator. This takes into consideration that the abdominal surgical procedure will also be performed on a child, thus smaller abdominal workspace. Hence, there is a need to determine an acceptable margin of interference with respect to a feasible distance between the stator sets for the system to perform effectively. With reference to Fig. 7 and Table III, since the interference onto R_1 at 20mm and 50mm inter-set distances do not differ significantly, the inter-set distance of 20mm can potentially be taken as the threshold of interference onto rotor R_1 as this is considered a reasonable distance between the sets, while other methods can be implemented to further suppress the interference. Following this, with the knowledge of the validated and accurate model presented in this paper, model-based controllers can be developed to address the unwanted magnetic interference caused by multiple stator sets to provide smooth actuation on the robotic surgical manipulator.

VI. Conclusion

The investigation of the magnetic interaction in a multi-DOF LEMA system with a neighbouring stator set was presented, based on the configuration which takes into account the abdominal workspace. The simulations implementing the magnetic field, static electromechnical and system dynamic models were performed to study the interference caused by a neighbouring set (i.e. stator set 2, S_{2j}) onto rotor, R_1. The speed responses of R_1 with two different references for stator set 2 (i.e. 30 rad/s and 100 rad/s) was obtained for the analysis as the angular velocity of the rotor shows the affect of the magnetic interference due to the S_{2j}. The simulation results are then compared against the speed responses obtained experimentally, which shows a good match, hence validating the accuracy of the dynamic model. The magnetic interference by S_{2j} onto R_1 was also investigated with the variation of distance between the stator sets to observe the reduction of the interference as the inter-set distance grows. Though it is desired to have the stator sets as far as possible to completely eliminate the interference, the constraints on the abdominal workspace has to be considered. Therefore, a feasible threshold was defined, leading to the establishment of a configuration specification for the multi-DOF LEMA in the aspect of inter-set distance, as well as the future work in developing model-based controllers (i.e. using the mathematical models validated) to further suppress the disturbances contributed by the neighbouring coils in the multi-DOF system setup.

References

[1] W. S. Richardson, K. M. Carter, G. M. Fuhrman, J. S. Bolton, and J. C. Bowen. Minimally invasive abdominal surgery. The Ochsner Journal, vol. 2, no. 3, pp. 153–157, 2000.

[2] S. Khandelwal, A. S. Wright, E. Figueredo, C. A. Pellegrini, and B. K. Oelschlager. Single-incision laparoscopy: training, techniques, and safe introduction to clinical practice. Journal of Laparoendoscopic & Advanced Surgical Techniques, vol. 21, no. 8, pp. 687–693, 2011.

[3] F. Leong, N. Garbin, C. DiNatali, A. Mohammadi, D. Thiruchelvam, D. Oetomo, and P. Valdastri. Magnetic Surgical Instruments for Robotic Abdominal Surgery. IEEE Reviews in Biomedical Engineering (RBME), vol. 9, pp. 66–78, Jan 2016.

[4] J. Cadeddu, R. Fernandez, M. Desai, R. Bergs, C. Tracy, S.-J. Tang, P. Rao, M. Desai, and D. Scott. Novel magnetically guided intraabdominal camera to facilitate laparoendoscopic single-site surgery: initial human experience. Surgical Endoscopy, vol. 23, no. 8, pp. 1894-1899, 2009.

[5] S. Park, R. A. Bergs, R. Eberhart, L. Baker, R. Fernandez, and J. A. Cadeddu. Trocar-less instrumentation for laparoscopy: magnetic positioning of intra-abdominal camera and retractor. Annals of surgery, vol. 245, no. 3, pp. 379–384, 2007.

[6] G. Tortora, M. Salerno, T. Ranzani, S. Tognarelli, P. Dario, and A. Menciassi. A modular magnetic platform for natural orifice transluminal endoscopic surgery. In Procs. IEEE International Conference of Engineering in Medicine and Biology Society (EMBS), pp. 6265-6268, 2013.

[7] K. Ikuta, S. Makita, and S. Arimoto. Non-contact magnetic gear for micro transmission mechanism. In Procs. IEEE Micro Electro Mechanical Systems (MEMS), pp. 125–130, 1991.

[8] C. Di Natali, J. Buzzi, N. Garbin, M. Beccani, and P. Valdastri. Closed-loop control of local magnetic actuation for robotic surgical instruments. IEEE Transactions on Robotics, vol. 31, no. 1, pp. 143-156, 2015.

[9] N. Garbin, C. Di Natali, J. Buzzi, E. De Momi, and P. Valdastri. Laparoscopic tissue retractor based on local magnetic actuation, Journal of Medical Devices, vol. 9, no. 1, p. 011005, 2015.

[10] A. Mohammadi, C. Di Natali, D. Samsonas, P. Valdastri, Y. Tan, and D. Oetomo. Electromagnetic actuator across abdominal wall for minimally invasive robotic surgery, Journal of Medical Devices, vol. 9, no. 3, p. 030937, 2015.

[11] G. Hang, M. Bain, J. Y. Chang, S. Fang, F. Leong, A. Mohammadi, P. Valdastri, and D. Oetomo. Local Magnetic Actuation Based Laparoscopic Camera for Minimally Invasive Surgery, Australasian Conference on Robotics and Automation, 2015.

[12] F. Leong, A. Mohammadi, Y. Tan, P. Valdastri and D. Oetomo. Experimentally Validated Modelling of Electromechanical Dynamics on Local Magnetic Actuation System for Abdominal Surgery, In Procs. Australasian Conference of Robotics and Automation, 2016.